JMEPEG (2024) 33:3613–3626
https://doi.org/10.1007/s11665-024-09144-9


1059-9495/$19.00

ORIGINAL RESEARCH ARTICLE

# Mechanical Characterization of Polylactic Acid, Polycarbonate, and Carbon Fiber-Reinforced Polyamide Specimens Fabricated by Fused Deposition Modeling

*Sotiria Dimitrellou, Isidoros Iakovidis, and Dimitrios-Rafail Psarianos*

Submitted: 13 November 2023 / Revised: 19 December 2023 / Accepted: 22 December 2023 / Published online: 22 January 2024

**This paper investigates the mechanical behavior of polylactic acid (PLA), polycarbonate (PC) and carbon fiber-reinforced high-temperature polyamide (PAHT-CF) specimens fabricated by fused deposition modeling (FDM). PC and PAHT-CF are considered engineering grade materials that exhibit good mechanical properties, suitable for rapid prototypes and functional parts fabrication. PLA, a popular, commonly used FDM material, has been included in this work for comparison purposes. The purpose of the present study is to provide comprehensive experimental data on the materials' critical properties since limited data is available in the existing literature and there is a lack of comparative analysis regarding the three materials. Mechanical characterization has been carried out on the basis of tensile, three-point bending, impact and creep tests. Measurements of hardness, density and porosity were conducted, and the specimens' morphology was examined through microscopy. The results showed that the highest strength and flexural modulus of elasticity were observed for the PAHT-CF specimens followed by PC and PLA. PC specimens exhibited the highest impact resistance followed by PAHT-CF and PLA. The highest stage II creep resistance was achieved by PAHT-CF followed by PC and PLA. The optical and scanning electron microscopy images revealed that specimens' quality depends on the printing parameters.**

**Keywords** additive manufacturing, fiber-reinforced composites, fused deposition modeling, mechanical testing, PAHT-CF, PC, PLA

## 1. Introduction

Additive manufacturing (AM) is a rapidly evolving technology which has the potential to replace conventional manufacturing technologies as it has the comparative advantage of reducing the production time and costs, generating high complicate geometries, and contributing to sustainability in terms of material and energy (Ref 1). AM can be utilized for the fabrication of prototypes, prototype tooling, functional components, and customized products. Material extrusion (MEX) is a generalized standard term for the additive manufacturing process in which material is selectively dispensed through a nozzle, and fused deposition modeling (FDM) is the commercial term used for material extrusion according to ISO/ASTM 52900. FDM is a very popular AM technique due to the printing process simplicity, the ability to manufacture complex objects with no waste of material, the application to a wide variety of materials, and its adaptability for industrial, commercial, or domestic usage (Ref 2, 3). In FDM technique the material in the form of solid filament is heated to its melting temperature and then extruded through a nozzle of specific diameter and deposited layer by layer on the built plate till the product is completely manufactured. The quality of the 3D-printed products, in terms of dimensional accuracy and surface roughness, and their mechanical properties are significantly affected by the process parameters selected for the printing process. According to observations of many researchers in the literature, some of the most critical FDM process parameters are layer height, infill density, infill pattern, extrusion temperature, build orientation, raster angle (also referred as deposition orientation), raster width and printing speed (Ref 4, 5).

In general, the mechanical behavior of the FDM printed parts can be improved by optimizing the process parameters or/and using a material filament with high strength. Materials that can be used in FDM nowadays are thermoplastic polymers, such as Acrylonitrile butadiene styrene copolymer (ABS), Polypropylene (PP), Polylactic acid (PLA), Polycarbonate (PC), Polyamide (PA), and Polyether ether ketone (PEEK), composites reinforced with continuous or discontinuous fibers, and blends of different polymers (Ref 2). The appropriate material is selected according to the final product requirements, the filament's physical and mechanical properties, and the available printing apparatus.

ABS is the most common semi-crystalline polymer used for FDM, with superior impact strength, but its tensile strength is lower than PLA. PP is a flexible material, chemical resistant, with low weight and lower tensile strength than ABS, but difficult to print as it induces warping and shrinkage and interlayer delamination (Ref 6). PEEK is a thermoplastic biomaterial with high thermal resistance and stability, and superior mechanical properties, however it is difficult to print due to high shrinkage and its high melting temperature (Ref 2).

**Sotiria Dimitrellou, Isidoros Iakovidis,** and **Dimitrios-Rafail Psarianos**, Department of Naval Architecture, School of Engineering, University of West Attica, Athens, Greece. Contact e-mail: sdimitre@uniwa.gr.

PLA is a very popular biodegradable polymer with low melting point, easy printing processability, stronger and stiffer than ABS and PP, but brittle and not applicable to high temperatures. PC is a high-performance polymer, with high tensile strength even when it is recycled, excellent toughness, very good thermal and dimensional stability (Ref 7). Different types of polyamides exist based on the form of the polymeric chains, with PA6, PA11 and PA12 being the most popular for 3D printing applications. PA6 has good flexibility and durability, higher tensile strength when compared to ABS and PLA, low creep, good resistance to impact, and improved mechanical properties at higher temperatures (Ref 8). However, due to its high crystallinity (as with PEEK and PP) and the generation of shrinkage stress, it presents high shrinkage and interlayer delamination during the printing process, and low-dimensional stability (Ref 6, 9). Some properties of the polymers can though be improved when they are combined with other materials to produce a composite. In fiber-reinforced composites (FRC), most research works utilize ABS, PLA and PA as the matrix material due to their low melting point, and fibers of carbon, glass or Kevlar to enhance the mechanical and physical properties of the pure polymer (Ref 2, 8, 10).

In the present study, the authors investigate the mechanical behavior of PLA, PC and PAHT-CF printed specimens. All three materials are commercially available and can easily be printed on an FDM 3D printer. PC is considered suitable for engineering applications that require reasonable strength and high thermal loads, as it maintains its structural integrity up to its glass transition temperature of 110 °C. High temperature PA reinforced with carbon fibers can withstand high mechanical stress and thermal stability up to 150 °C and can be used for tough environments in demanding engineering applications. PLA is the third material used in the investigation, to perform as a basis for the comparison of the experimental values, considering that all specimens are printed in the same 3D printer with common process parameters and environmental conditions. ABS and PA were excluded from this study due to their poorer properties, that restrict their application in many engineering applications. The investigation includes experimental tests of the tensile strength, flexural modulus of elasticity, impact strength and creep rate, as well as hardness, density and porosity measurements. Optical and scanning electron microscopy (SEM) observations on the morphology of the specimens are also provided.

The rest of the paper is organized as follows. In section 2 a short review of the recent literature concerning the considered materials is presented. Section 3 refers to the materials and methods, and section 4 presents the experimental results and the discussion. The last section summarizes the conclusions.

## 2. Recent Progress in the Characterization of FDM Printed Samples

In the literature, a great number of scholars have conducted research to experimentally investigate the physical and mechanical properties of FDM printed samples. The methodology usually involves the investigation of the effect of different printing process parameters on the performance of a single polymer material, pure or reinforced. PLA printed specimens have been extensively examined for tensile strength (Ref 11-14), flexural strength (Ref 11, 15, 16), impact strength (Ref 17-19), hardness (Ref 12, 19-21), and creep (Ref 22, 23). PC printed specimens have been examined for tensile strength (Ref 24-28), flexural strength (Ref 26, 28), impact strength (Ref 24-26, 28), hardness (Ref 25, 26), compressive strength (Ref 7, 28), and creep (Ref 29). PA-CF printed specimens have been examined for tensile strength (Ref 6, 30-33), flexural strength (Ref 30, 32-34), impact strength (Ref 32, 34, 35), compressive strength (Ref 33), and creep (Ref 31, 36).

The results of these studies depend on the user-selected process parameters (optimized or common) and the environmental conditions during the printing process of a specific material and cannot provide a reliable comparison of the mechanical properties for different materials. In this context, researchers have performed studies related to the mechanical characterization and comparison of different 3D printing materials, either considering or not the effect of the process parameters in the experimental results. Table 1 gives the summary of the latest relative literature.

The present research work investigates the mechanical behavior of three different materials (PLA, PC, PAHT-CF) produced by the FDM printing technique. The contribution of this study is the following:

i. The paper investigates the more critical mechanical properties in engineering applications (tensile, flexural, impact, creep), and performs hardness, density and porosity measurement, providing a thorough and comprehensive comparison of the three materials' behavior.
ii. The materials are produced and tested under similar conditions (same commercial 3D printer, common FDM process parameters, realistic temperature and humidity conditions), and the experimental results can be useful as a baseline for knowledge and relative sound judgment.
iii. There is a lack of comparative analysis between PAHT–CF, PC and PLA in the existing literature, indicating the necessity for this study, as PAHT–CF and PC are considered potential materials for high temperature engineering applications.
iv. Literature is not yet enriched enough with experimental data relative to the creep behavior of PAHT-CF, PC and PLA. Only one study (Ref 43) has been found that compares the creep behavior of different FDM materials (PAHT-CF is not included).
v. To the knowledge of the authors, no experimental data regarding the creep rate and hardness of PAHT-CF (15% carbon fiber-reinforced high temperature PA6) has been reported before in literature. Tutar et al. (Ref 33) present the effect of process parameters on the tensile, compressive and flexural behavior as well as the porosity of PAHT-CF, and Condruz et al. (Ref 49) compare the tensile and flexural properties of tough PLA, nGen CF 10 and PAHT-CF.
vi. The outcome of this work can provide a better understanding from an engineering perspective of the physical and mechanical behavior of the three materials fabricated with common FDM process parameters in realistic environmental conditions.

**Table 1 Summary of studies related to the mechanical characterization and comparison of FDM printing materials.**

| Studies | Mechanical and physical properties (process parameters) | Materials |
|---|---|---|
| Tanikella et al. (Ref 37) | Tensile, density (N/A) | Ninjaflex, SemiFlex, HIPS, T-Glase, PC, Nylon Bridge, Nylon 618, ABS |
| Lay et al. (Ref 38) | Tensile, impact, density, viscosity, water absorption (N/A) | PLA, ABS, Nylon 6 |
| Kannan et al. (Ref 39) | Tensile, Young's modulus, vibration | ABS, PC, PC-ABS |
| Vidakis et al. (Ref 40) | Tensile | PLA, ABS, PETG, PA6, PP |
| Arunkumar et al. (Ref 41) | Tensile, flexural, impact (infill density) | PLA-CF, PA-CF |
| García-León et al. (Ref 42) | Impact (printing speed, layer height, infill density) | PC, PA-CF |
| Dogan (Ref 43) | Creep (ambient temperature, stress level) | ABS, CPE, PLA, Tough PLA PC, Nylon |
| Frohn-Sörensen et al. (Ref 44) | Bending, compression, surface roughness, Shore D hardness, density (layer height and number of walls) | PC, PLA, PA, PETG |
| Rodríguez-Reyna et al. (Ref 45) | Tensile, modulus of elasticity (pattern, infill percentage, printing direction, layer height) | PLA, ABS, Nylon-CF |
| Palacios et al. (Ref 46) | Shore A and Shore D hardness (N/A) | ABS, PLA, PC, NYLON, PETG, ABS-CF, PLA-CF, PC-CF, NYLON-CF, PETG-CF |
| Venkatesh et al. (Ref 47) | Tensile, Young's modulus (deposition orientation) | PLA, ABS, NYLON, PLA-CF, ABS-CF, NYLON-CF |
| Yankin et al. (Ref 48) | Tensile (infill pattern, infill density, printing speed) | ABS, NYLON |
| Condruz et al. (Ref 49) | Tensile, flexural (raster orientation) | Tough PLA, nGen CF10, PAHT CF15 |

## 3. Materials and Methods

### 3.1 Materials Specification

The materials used in the present experimental study are PLA and PC, supplied from Ultimaker (Zaltbommel, the Netherlands), and Ultrafuse PAHT-CF, supplied from BASF (Emmen, The Netherlands), all with a filament diameter of 2.85 mm. Ultimaker PLA filament is made from organic and renewable sources and is characterized by good tensile strength and surface quality, and very good processability. PLA was chosen to provide a proper comparative evaluation for the samples printed and tested under similar conditions, as it is one of the most accepted materials in 3D printing. PC was selected because it is a polymer widely used in engineering applications and has been reported to possess high mechanical properties. According to supplier, Ultimaker PC is characterized by high toughness, strong interlayer bonding and good bed adhesion, and retains dimensional stability when subjected to temperatures as high as 110 °C. Ultrafuse PAHT CF15 is a PA6-based copolymer with 15 % short carbon fibers. It was selected as it is considered a high-temperature engineering grade filament with advanced mechanical properties, low water absorption, good dimensional stability, and high temperature resistance up to 150 °C. Also, carbon fibers add stability and rigidity to the polyamide matrix reducing warping or clogging during the printing process. The mechanical properties of PLA, PC and PAHT-CF as specified by the suppliers are summarized in Table 2.

### 3.2 Printing Process of the Test Specimens

The specimens were 3D modeled using the Autodesk Fusion360 software. Their dimensions were determined considering the standards for tensile test (ISO 527-2, ASTM D638), three-point bending test (ASTM D790), Izod impact test (ISO 180:2019, ASTM D256) and creep test (ASTM D2990, ISO 899) and were appropriately modified as shown in Fig. 1. The thickness of the tensile, flexural and creep test specimens were set to 3 mm.

The stereolithography (.stl) files of the 3D models were transferred to Ultimaker Cura 4.12.1 software where the printing settings were set and the G-code for the extruder head's movements was generated. The selection of the printing process parameters was based on the default values set for each material by the Cura software, the suppliers' printing guidelines, previous printing tests by the authors, and standard accepted values reported in the literature. Table 3 summarizes the selected process parameters for the three materials.

All specimens were printed in a commercial FDM 3D printer (Ultimaker S5) in *XY* flat build orientation, as shown in Fig. 2, with a layer height of 0.15 mm and infill density of 100%. To improve adhesion to the glass build plate and minimize shrinkage and wrapping, a thick layer (raft base) was applied below the models for PLA and PAHT-CF materials. The infill density of the specimen was set to 100% in order to support the maximum possible mechanical loads.

Flat build orientation on *XY* plane was selected for the specimens, considering that most studies in the literature indicate that tensile properties are maximized at 0° build orientation, mainly because the filaments are deposited parallel to the direction of the applied load (Ref 4, 50). However, the flat built orientation may not provide better results for other mechanical properties when the loads are applied to other directions. The triangular pattern was selected for the 100% infill density, as shown in Fig. 3(a), as it is quite popular, among the available patterns, for its medium complexity, lower printing times, strong structure, and maximum infill pattern size (Ref 19, 51, 52). However, the infill pattern parameter mainly affects the properties when parts are printed at a low infill density. Deposition orientation was set to 45/135° for the top and bottom layers (Fig. 3b), as it has been reported in several studies that the 45/135° raster angle can show slightly higher tensile and impact strength values compared to those of 0/90° (Ref 45, 47, 50).

### 3.3 Testing Methods and Equipment

The tensile strength of the manufactured specimens was determined using a universal testing PWYWE machine with a load cell capacity of 10 kN, at a constant crosshead displacement of 2 mm/min. During the test, the load applied to the specimen gradually varied until the failure point of the specimen and the elongation was recorded by a Force-length meter (model: Kraft–WegmeBgerät, PWYWE). The experimental stress–strain curves were obtained for the specimen and ultimate tensile stress (UTS) and elongation at break were calculated. Two specimens were tested for each material, and the results were obtained by averaging the data.

The impact strength was measured by an Avery–Denison impact testing machine equipped with a 2.5 kg pendulum arm and a built-in dynamometer that records the energy of fracture at a range from 0 to 15.0 Joules. The Izod method was used for the experimental determination of the impact strength of the specimens. The arm was raised to an initial height of 610 mm

**Table 2 Mechanical properties specified by the suppliers.**

| Mechanical property | PLA | PC | PAHT-CF |
|---|---|---|---|
| Tensile stress at break (MPa) (ISO 527) | 45.6 | 53.7 | 62.9 |
| Tensile Modulus (GPa) (ISO 527) | 2.35 | 1.90 | 5.05 |
| Elongation at break (%) (ISO 527) | 5.2 | 5.9 | 2.9 |
| Flexural strength (MPa) (ISO 178) | 103 | 95.5 | 125.1 |
| Flexural Modulus (GPa) (ISO 178) | 3.15 | 2.31 | 6.06 |
| Density (kg/m$^3$) | N/A | N/A | 1203 |
| Specific gravity | 1.24 (ASTM D1505) | 1.18-1.20 (ASTM D792) | N/A |
| Shore Hardness D | 83 (Durometer) | 80 (Durometer) | 72 (ISO 7619-1) |
| Impact strength (kJ/m$^2$) (ISO 180—Izod) | 5.1 (notched) | 14.8 (notched) | 6.5 (notched) 16.3 (unnotched) |

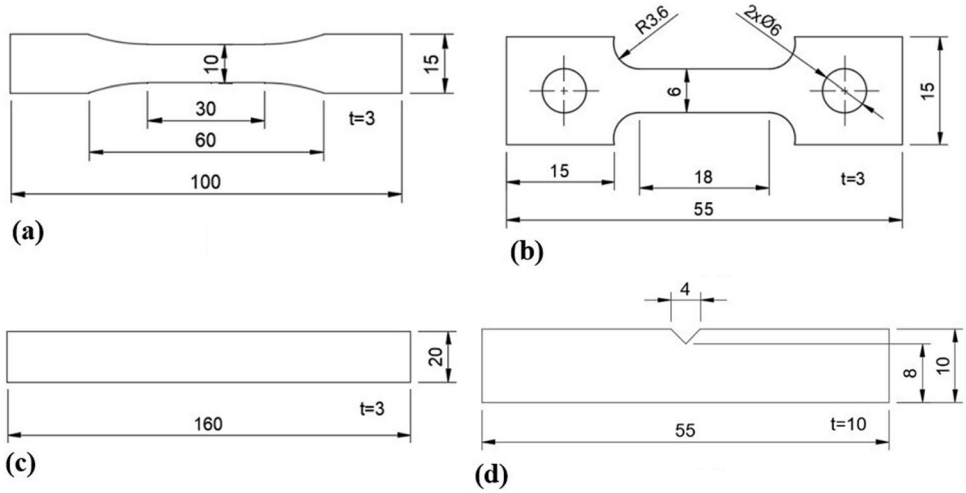


**Fig. 1** Dimensions of specimens for (a) tensile test; (b) creep test; (c) three-point bending test; (d) impact test

**Table 3 Printing process parameters.**

| Parameter | PLA | PC | PAHT-CF |
|---|---|---|---|
| Layer height (mm) | 0.15 | 0.15 | 0.15 |
| Raster width (mm) | 0.38 | 0.40 | 0.58 |
| Number of walls | 3 | 3 | 3 |
| Wall thickness (mm) | 1 | 1.2 | 1.7 |
| Number of top layers | 3 | 3 | 3 |
| Number of bottom layers | 3 | 3 | 3 |
| Top/bottom thickness (mm) | 1 | 1.2 | 1 |
| Infill density (%) | 100 | 100 | 100 |
| Infill pattern | Triangles | Triangles | Triangles |
| Build orientation | *X-Y* | *X-Y* | *X-Y* |
| Deposition orientation | 45°/135° | 45°/135° | 45°/135° |
| Printing speed (mm/sec) | 70 | 70 | 70 |
| Extrusion head type | AA 0.4 mm | AA 0.4 mm | CC 0.6 mm |
| Printing temperature (°C) | 200 | 280 | 260 |
| Build plate temperature (°C) | 60 | 110 | 100 |
| Built plate adhesion type | Raft | … | Raft |
| Raft material | PLA | … | BVOH |

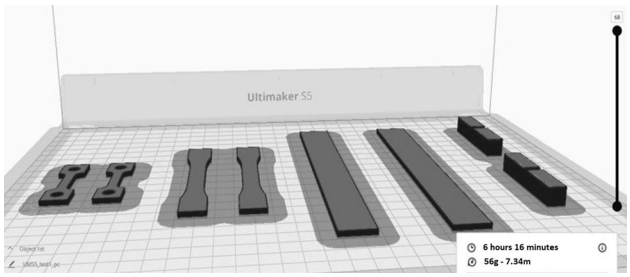


**Fig. 2** Flat *X-Y* build orientation and built plate adhesion (raft base) for the test specimens

and then released swinging downwards and struck the specimen at impact speed of 3.46 m/s. Impact strength was calculated according to ISO 180:2019 as the absorbed energy per unit of the fractured cross-sectional area of the specimen. Two notched specimens were tested for each material, and the results were obtained by averaging the data. The fracture surface of the samples was then inspected and characterized.

The flexural test was applied according to ASTM D790 using a three-point loading testing device with a span length of 80 mm between the two supports. Different loads were applied vertically to the center of the specimen and the corresponding maximum deflection in mid-span was recorded. The flexural modulus of elasticity $E_B$ was calculated as the slope of the stress–strain curves corresponding to elastic flexural deformation.

Creep is the time-dependent deformation of a material under a constant load in a specified temperature and indicates its durability and dimensional stability during operation. Creep tests of the specimens were performed using an Edibon EEFCR creep testing machine under a constant load of 35 Kg. Temperature in the closure test area was set to 44 ± 2 °C for PLA, 41 ± 3 °C for PC, and 45 ± 2 °C for PAHT-CF15 specimen. The specified temperature level was controlled by a heater that started operating immediately after a temperature drop of 1 degree. A built-in analogue micrometer was used to measure the creep elongation and the values were recorded every 30 s. Strain versus time curves were derived for creep stage I and stage II.

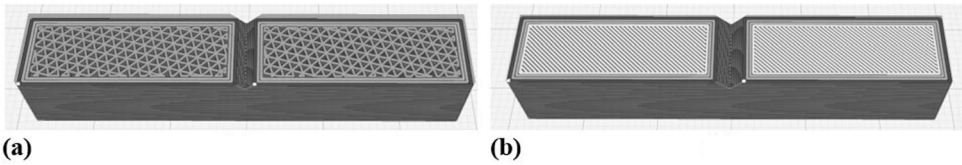


**Fig. 3** Schematic view of impact test specimens with (a) triangular pattern for the 100% infill; (b) raster angle of 135° for the top layer

Hardness measurements were carried out according to standard ISO 868:2003 using an analogue Shore D durometer (model: Sauter HBD 100-0) with a conical 30° indenter, depth of indentation 0-2.5 mm, and test pressure of 50 N. Three surfaces were examined for each specimen: the top surface which was wet grinded using a Struers Silicon Carbide Paper #4000 in a Struers LaboPol-5 device, the surface of the vertical side of the specimen that is defined in 3D printing as "wall", and the bottom surface of the sample that was in contact with the printer's glass build plate. The test was repeated at five different points on each surface.

Density measurements were performed according to the standard ASTM D792 buoyancy method. A single piece of each sample weighing 3 − 4 g was initially weighed in air and subsequently fully immersed in deionized water using an appropriate suspension device and an analytic balance with a precision of 0.001 g. The process was repeated for 3-5 different pieces of each material and the density values were averaged. Equation 1 was used to calculate the density in each case:

$$d = d_w \cdot \frac{m_3 - m_1}{(m_3 - m_1) - (m_4 - m_2)} \quad \text{(Eq 1)}$$

where $d_w$ is the density of water in g/cm$^3$, $m_1$ is the mass of the wire in the water, $m_2$ is the mass of the wire in the water, $m_3$ is the mass of the sample in the air, and $m_4$ is the mass of the sample immersed in water.

The porosity $P$ of the fabricated specimens was also calculated as a % percentage, according to Eq 2:

$$P = 100 \cdot \left(1 - \left(\frac{d_{\text{exp}}}{d_{\text{theor}}}\right)\right) \quad \text{(Eq 2)}$$

where $d_{\text{exp}}$ is the experimental and $d_{\text{theor}}$ is the theoretical density of the material as provided by the supplier.

## 4. Results and Discussion

### 4.1 Dimensional Accuracy

The dimensional accuracy of FDM printed parts is affected by a variety of factors, including the filament's physical properties, such as moisture absorption and thermal expansion, and the printing process parameters, such as printing temperature, printing speed, layer height and deposition orientation (Ref 4, 19, 53). The degree of moisture absorption depends on the type of material and the environmental conditions during its storage and testing. According to the literature, PC has the lowest water absorption capability of the investigated plastics, PLA follows, and PA6 is the most absorbent due to its hygroscopic nature (Ref 38, 54). In the present study the filaments were not dried before printing, and this could be one of the reasons for the dimensional deviations of the 3D printed specimens. The coefficient of linear thermal expansion determines the change in size of a material due to temperature variations. Polymers exhibit a high coefficient of thermal expansion which can be thus reduced by the reinforcement of the matrix with carbon fibers.

**Table 4 Measured dimensions of the FDM printed specimens.**

| Specimen | Length | Width | Thickness |
|---|---|---|---|
| *Tensile CAD* | *100.00 mm* | *10.00 mm* | *3.00 mm* |
| PLA | 100 + 0.50 | 10 + 0.20 | 3 + 0.30 |
| PC | 100 + 0.80 | 10 + 0.59 | 3 + 0.04 |
| PAHT-CF | 100 + 0.88 | 10 + 0.65 | 3 + 0.24 |
| *Flexural CAD* | *160.00 mm* | *20.00 mm* | *3.00 mm* |
| PLA | 160 + 0.30 | 20 + 0.15 | 3 + 0.30 |
| PC | 160 + 0.50 | 20 + 0.70 | 3 + 0.00 |
| PAHT-CF | 160 + 0.70 | 20 + 0.60 | 3 + 0.24 |
| *Creep CAD* | *55.00 mm* | *6.00 mm* | *3.00 mm* |
| PLA | 55 + 0.36 | 6 + 0.27 | 3 + 0.40 |
| PC | 55 + 0.55 | 6 + 0.67 | 3 + 0.05 |
| PAHT-CF | 55 + 0.83 | 6 + 0.69 | 3 + 0.34 |
| *Impact CAD* | *55.00 mm* | *10.00 mm* | *10.00 mm* |
| PLA | 55 + 0.30 | 10 + 0.30 | 10 + 0.30 |
| PC | 55 + 0.20 | 10 + 0.45 | 10 + 0.20 |
| PAHT-CF | 55 + 0.90 | 10 + 0.80 | 10 + 0.20 |

The dimensional measurements of the 3D printed specimens were carried out using a micrometer with a precision of 0.01 mm, and the obtained dimensions were compared to the given dimensions (CAD) in Table 4. In all cases there was a positive deviation in the size of the printed specimens in all three dimensions.

Regarding the *Z*-axis dimension (specimen's thickness), PC was characterized by the highest dimensional stability in all samples followed by PAHT-CF. The highest deviations in thickness were measured for the PLA specimens.

Regarding the dimensions in the *X-Y* plane (length and width) PLA appeared to be the most stable material. Comparing the other two materials, the observations vary according to the specimen's thickness. For the tensile, flexural and creep specimens (3 mm thickness), PC showed a slightly better accuracy in length and width than PAHT-CF. Regarding the impact test specimens (10 mm thickness), PAHT-CF exhibited a significantly larger deviation in length and width, compared to PLA and PC. In general, it can be observed that PAHT-CF did not show the expected, according to supplier's specifications, dimensional stability in X and Y direction. The reason may be a very high printing temperature together with a high printing speed. The high printing speed did not permit the molted material to cool before a new layer was deposited and the high nozzle temperature overheated the extruded material. As the deposition process was repeated constantly for a greater number of layers, the printing beads, also known as rasters or

strands, were created thicker expanding the layer size beyond the given dimensions in *XY* plane.

### 4.2 Mechanical Properties

Stress–strain curves obtained from the uniaxial tensile testing of the specimens are depicted in Fig. 4. Two specimens were tested for each material. The mean (average) values of the tensile properties were derived, and the highest ultimate tensile strength (UTS) was obtained for PAHT-CF, i.e., 81.5 MPa, followed by PC, i.e., 53.3 MPa, and PLA, i.e., 36.0 MPa. The superior UTS of PAHT-CF is attributed to the higher tensile properties of the reinforcement, i.e., carbon fibers incorporated in the polyamide matrix. Standard deviation values were calculated to be 2.7 for PLA, 1.9 for PC and 2.0 for PAHT-CF, indicating that PLA is more sensitive regarding the printing process and PC the most consistent material for FDM printing in terms of repeatability. The small slope of the stress-strain curve of PLA and PC (see Fig. 4) correspond to low Young's modulus values indicating restricted elastic behavior of these plastics compared to PAHT-CF. PC exhibits the highest elongation at break, determined as total (elastoplastic) or pure plastic uniaxial deformation. The tensile strength of the 3D printed specimens was 21% lower for PLA, 29% higher for PAHT-CF and almost the same for PC, compared to the values given by the suppliers (Table 1). These differences are due to the different printing process parameters, such as nozzle temperature, infill density, layer height, etc.

The stress-strain diagrams obtained from a three-point elastic bending test of the specimens are shown in Fig. 5. The higher flexural modulus of elasticity, i.e., 4.9 GPa was observed for PAHT-CF. It can be asserted that, although the flexural modulus of PA is lower than PLA and PC as has been reported in the literature (Ref 44), the addition of carbon fibers to the PA matrix significantly enhances the flexural behavior of the composite PAHT-CF and results in a higher flexural strength compared to PLA and PC. Regarding the other two materials, PC showed a higher flexural modulus, i.e., 2.1 GPa, than PLA, i.e., 1.9 GPa, indicating that PC is subjected to less deformation when the same bending load is applied.

To determine the impact resistance behavior of the specimens, the energy absorbed during the experiment was measured. PLA absorbed the less energy, i.e., 0.2 J, followed by PAHT-CF, i.e., 1.1 J, and PC, i.e., 1.2 J. All specimens exhibit brittle fracture with some degree of ductility upon impact. Impact strength was then defined as the absorbed energy per unit cross-sectional area of the specimens. A fracture toughness of 14.1 kJ/m$^2$ was determined for PC, followed by a value of 12.7 kJ/m$^2$ for PAHT-CF, and 2.3 kJ/m$^2$ for PLA. PLA and PC experimental values were similar to the impact strength values reported in the supplier' specifications (Table 1). However, the 3D printed PAHT-CF specimens exhibited a much higher impact strength compared to the supplier's specified value for notched specimens and slightly lower than the value for unnotched specimens.

Figure 6 shows the path of crack propagation and the fracture surface, generated through the impact test of the notched specimens. The impact loading was applied in a vertical direction to the build orientation. As can be seen, the path of the crack propagation of the PC specimen is straight, while for the PAHT-CF specimen a cup and cone type of fracture was observed indicating a more ductile material.

In general, the impact resistance and fracture toughness of a material increases by a stronger bonding of the interlayer structure and the absence of voids. Although the 3D printed PAHT-CF specimens exhibited low density and high porosity, as summarized in Table 5, it can be asserted that the presence of carbon fibers has enhanced its impact resistance. This occurs because the orientation of the carbon fibers is mostly perpendicular to crack propagation direction acting as a barrier able to

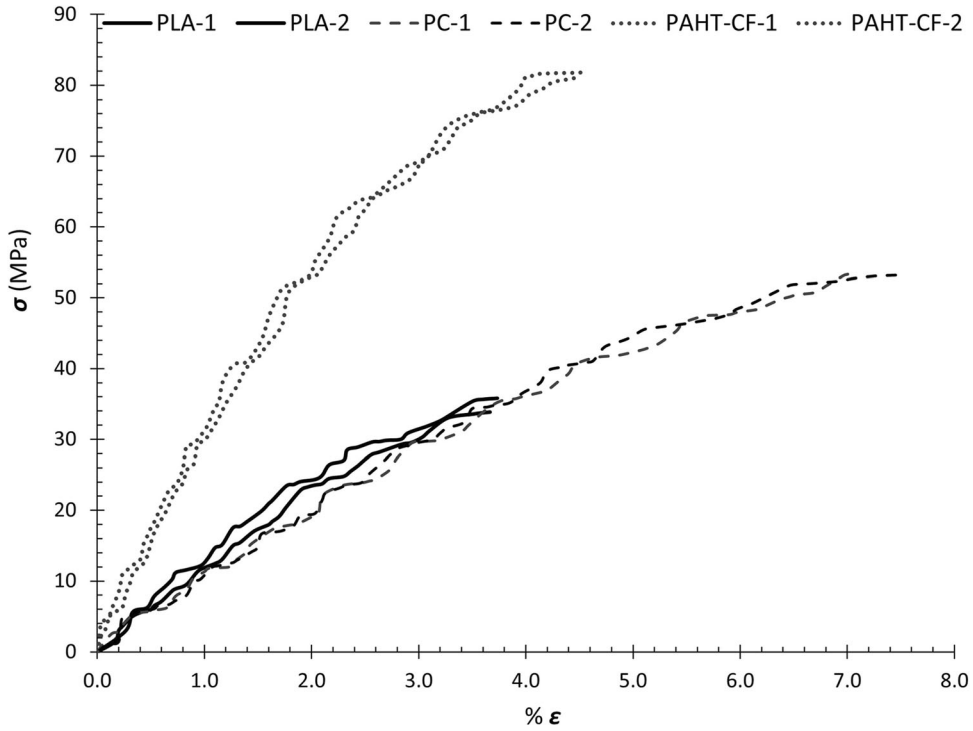


**Fig. 4** Stress–Strain curves of the tensile test specimens: PLA (solid line); PC (dashed line); PAHT-CF (dotted line)

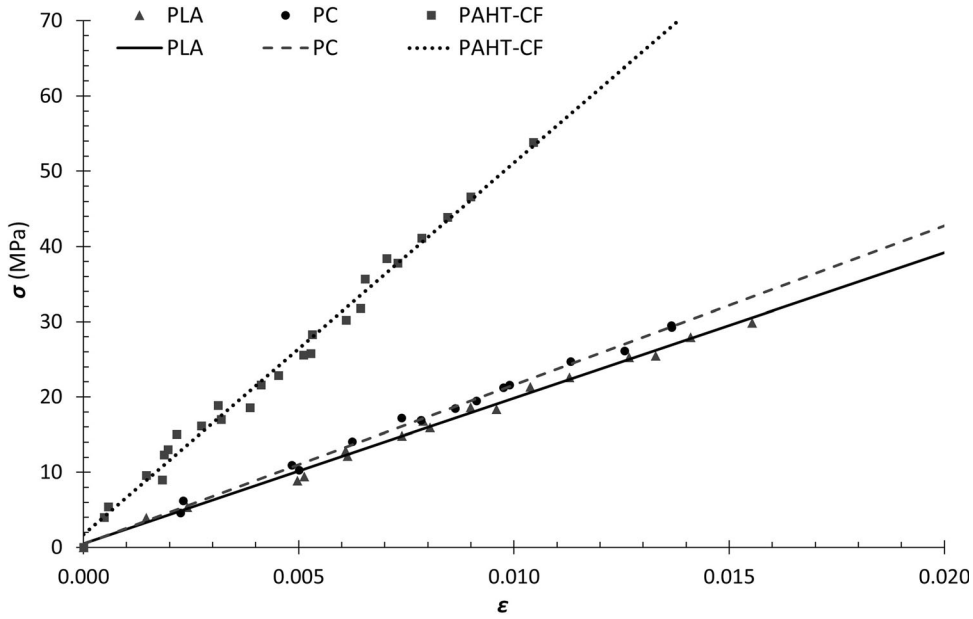


**Fig. 5** Flexural elastic behavior of the specimens subjected to the 3-point bending test: PLA (solid line); PC (dashed line); PAHT-CF (dotted line)

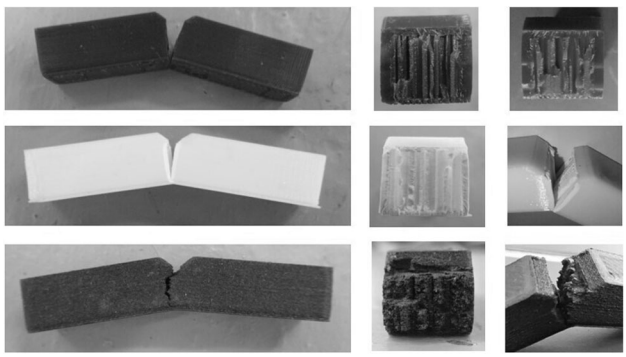

**Fig. 6** Tested 3D printed impact specimens: PLA (top); PC (middle); PAHT-CF (bottom)

prevent it. Furthermore, reinforcement with 15% carbon fiber is considered a sufficient percentage that strengthens the matrix, increasing the impact strength of the material. Similar results have been presented in (Ref 55).

Figure 7 illustrates the creep test results for the specimens under a constant tensile load of 35 Kg applied for 60 min at a predetermined temperature. The creep stages I and II were clearly observed, while the creep stage III did not occur under the testing conditions for any of the specimens. During stage I the elongation rate increases sharply first and then gradually drops, reaching a constant value at the end of stage I. During stage II, the elongation increases roughly linearly with time.

Although all materials exhibited a permanent and stable deformation, no rupture was achieved within the 60-minute testing time. According to the experimental results, PAHT-CF exhibited the highest stage II creep resistance. That means that PAHT-CF is the strongest material, compared to the others, under a constant applied load over time and its creep behavior is little affected when operating at a higher temperature than the ambient (45 °C in this study). PAHT-CF also showed the lower creep rate in stage II, which was retained for a longer time, followed by PC and PLA. In stage II, the elongation over time for PAHT-CF remained almost constant. The superior creep behavior of PAHT-CF, compared to PLA and PC, may be due to the reinforcement of the polyamide matrix with 15% carbon fibers. However, the FDM process parameters that affect the creep behavior of 3D printed PA-CF samples have not been studied extensively in the literature.

The hardness of 3D printed parts depends on the process parameters, mainly the build orientation, the raster angle, the nozzle temperature, the infill density, and the printing speed (Ref 19). Shore D hardness was measured on three surfaces of the impact specimen: the top surface which was wet grinded, the side surface and the bottom surface. The test was repeated at five different points on each surface, and the mean values are presented in Fig. 8.

The highest average hardness value was measured for PLA, followed by PC and PAHT-CF. Although the addition of carbon fibers to the PA matrix significantly enhances the hardness of pure PA, the hardness of PAHT-CF did not exceed the hardness of PLA and PC. The higher hardness value of PLA indicates that it is more brittle in comparison to PC and PAHT-CF which were found to be more ductile with respect to fracture. According to the experimental results, the hardness values of PLA and PC were found to be slightly higher than the values specified by the suppliers (Table 1), while the hardness of PAHT-CF was found to be 9.5% higher. This can be attributed to a considerably high printing temperature for PAHT-CF which increased the specimens' hardness. This is consistent with similar observations reported in the literature (Ref 13, 19).

The measured density of the PLA, PC and PAHT-CF specimens were found to be lower than the values specified by the suppliers by 9.0%, 2.6% and 10.4%, respectively. The main reason for the reduction in the density of FDM 3D printed specimens is the extended void volume (porosity) produced during the printing process. Voids are generated between the printing beads (inter-bead voids or raster gaps), and their size depends on certain process parameters, such as raster width,

**Table 5 Experimentally determined mechanical properties of the specimens**

| Mechanical property | PLA | PC | PAHT-CF |
|---|---|---|---|
| Tensile stress at break (MPa) | 36.0 | 53.3 | 81.5 |
| Total elongation at break (%) | 3.75 | 7.28 | 4.50 |
| Plastic elongation at break (%) | 1.21 | 2.75 | 1.78 |
| Flexural Modulus (GPa) | 1.9 | 2.1 | 4.9 |
| Density (g/cm$^3$) | 1.127 | 1.159 | 1.078 |
| Porosity (%) | 9.1 | 2.6 − 11.5 | 12.4 |
| Hardness (Shore D) | 84.5 | 82.7 | 79.7 |
| Impact strength (Izod, notched) (kJ/m$^2$) | 2.3 | 14.1 | 12.7 |
| Creep rate of stage II under a load of 35 Kg (x1000 mm/min) | 1.6 (at 44 °C) | 0.8 (at 41 °C) | 0.2 (at 45 °C) |

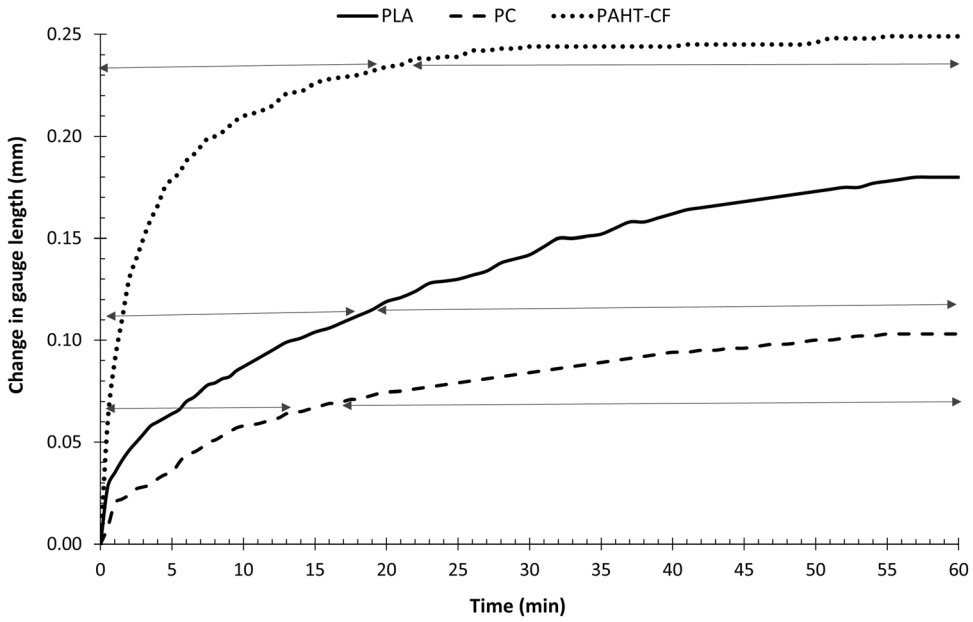


**Fig. 7** Creep behavior under a constant tensile load of 35 Kg: PLA at 44 °C (solid line); PC at 41 °C (dashed line); PAHT-CF at 45 °C (dotted line)

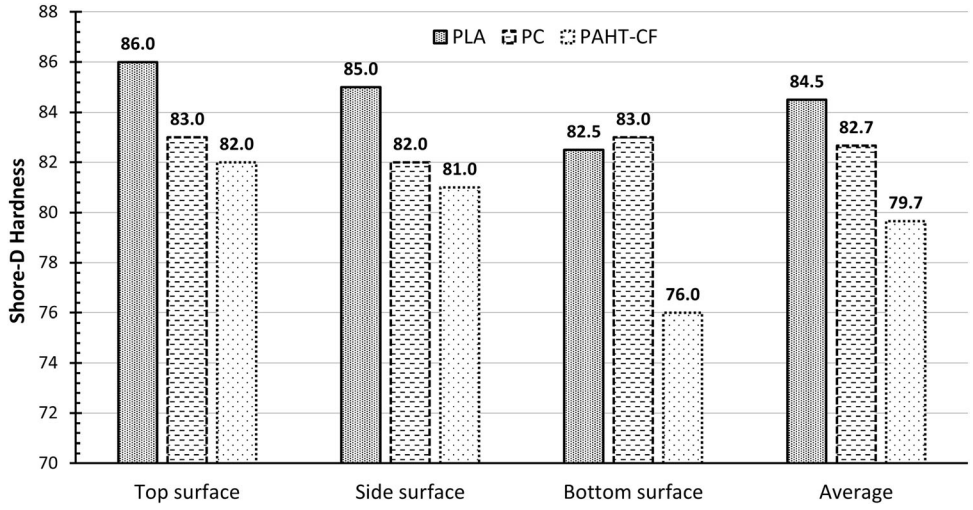


**Fig. 8** Shore D hardness of 3D printed specimens

layer height, nozzle temperature, printing speed, and infill pattern (Ref 56, 57). Also, pores can already exist within the filament and remain within the printing beads after deposition (intra-bead voids), especially in fiber-reinforced filaments due to the uneven distribution of fibers in the matrix. According to measurements, the lowest density of 1078 kg/m$^3$ and the higher porosity of 12.4% was obtained for the PAHT-CF specimens. By selecting a larger raster width or a lower printing speed the porosity in the specimen could have been reduced, leading to stronger adhesion and improved mechanical properties, as have been reported in the relative literature (Ref 56).

The critical properties of PLA, PC and PAHT-CF experimentally determined are summarized in Table 5.

### 4.3 Surface Morphology

One of the limitations of the FDM process is the presence of surface irregularities on the 3D printed parts which are affected by the process parameters and mainly occur due to the side-by-side line effect and the layer-by-layer deposition process. To investigate the surface morphology of the FDM printed specimens, optical and SEM images of the impact test specimen's upper surface, side surface and the fracture surface were recorded. They were acquired using a Labor-Lux MI5, Leitz optical microscope, an OPTIKA SZR stereo microscope, and a JEOL JSM-6390 scanning electron microscope. Representative images are shown in Fig 9, 10, 11, 12, and 13.

Figure 9(a) and (b) shows the upper surface (top layer) of the PLA and PC specimens, where the melted material has been deposited by the line-by-line arrangement. The deposition orientation at 135° can be clearly observed and it is possible to see some gaps, shown in black color, between the printing beads. These gaps inevitably occur during the FDM process. As the material is deposited, air gaps, also known as raster gaps, are created between the adjacent printing beads. In this study, the selection of the line pattern for the top-bottom layers and the setting of a high overlap between the adjacent beads in the deposition direction, resulted in a consistent flat top surface.

Some micropores are also visible on the surface of the PLA and PC samples in the images shown in Fig. 9(a) and (b). In the PC specimen, pores are more uniformly dispersed and have an almost cyclical shape, while in the PLA specimen they are irregular in shape. Pores are a common characteristic in FDM printed samples. These pores could be already present within the filament or could have been formed due to the uneven fusion of the material during the extrusion of the filament and the deposition of non-uniform molten material.

Figure 9(d) and (e) shows that the printing beads of PLA and PC specimens have not deposited quite straight, and the raster width is not the same along the printing path. The most common cause for this issue is a possible slight change in the temperature of the extrusion material that resulted in inconsistent flow and the extrusion of a raster that was wider or narrower in some sections. Some minor ridges can also be noticed, shown in white color, at the deposition direction of the printing beads. Concerning the PAHT-CF material (Fig. 9c and f) the deposition orientation at 135° can be clearly observed, but the adjacent printing beads are difficult to distinguish. Some gaps between the printing beads are visible (shown in darker color), however they appear smaller compared to the PLA and PC optical images.

In Fig. 10 the layer-by-layer deposition of the material can be clearly observed on the side surface of the PLA and PC specimens. The melted material seems to have been uniformly deposited and all individual layers exhibit the same height. The white lines are interlayer ridges that are created between the layers during the FDM deposition process and can further be reduced in size by setting a lower layer height. However, the printing process parameters selected in this study resulted in a rather smooth surface of fine quality for PLA and PC specimens, which can also be observed in Fig. 6.

SEM images of the side surface of the PAHT-CF impact test specimen are provided in Fig. 11. The individual layers can be

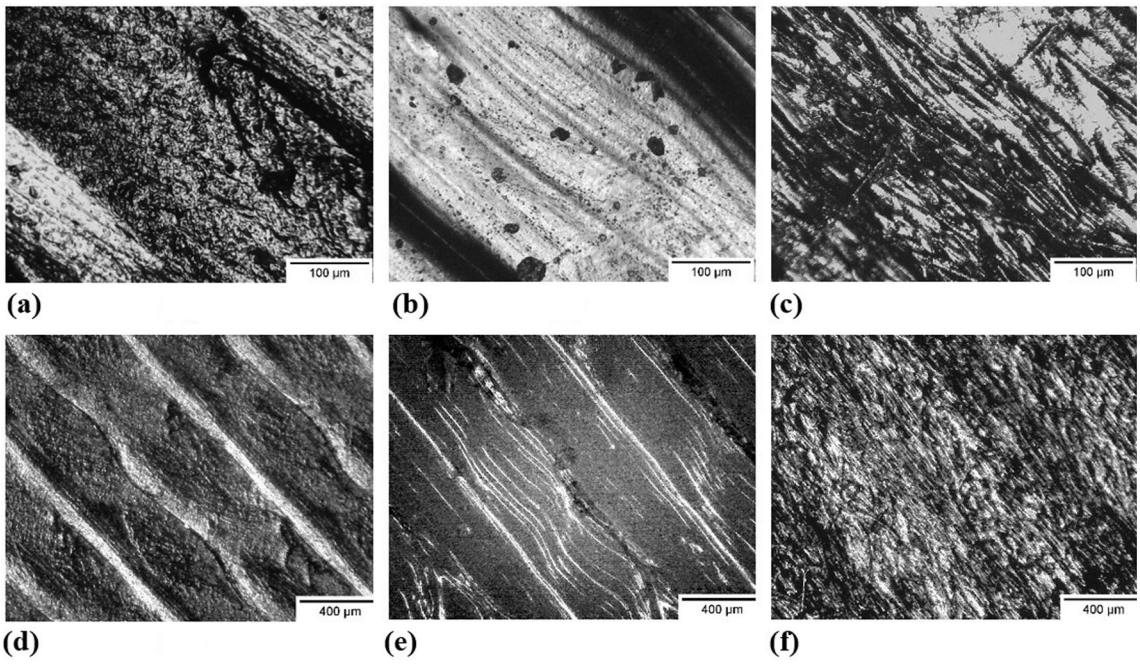


**Fig. 9** Optical images of the upper surface of the specimens: PLA (left); PC (middle); PAHT-CF (right)

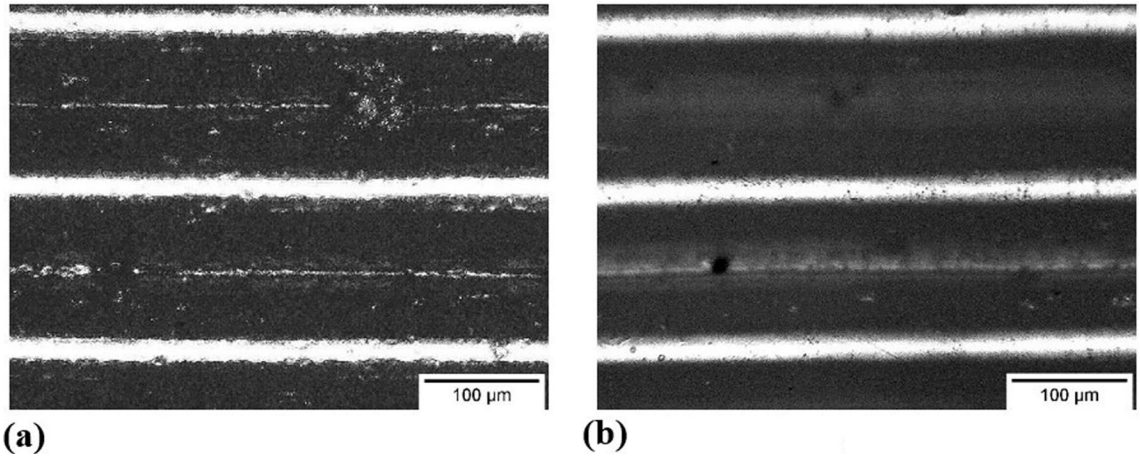


**Fig. 10** Optical images of the side surface of the specimens: (a) PLA; (b) PC

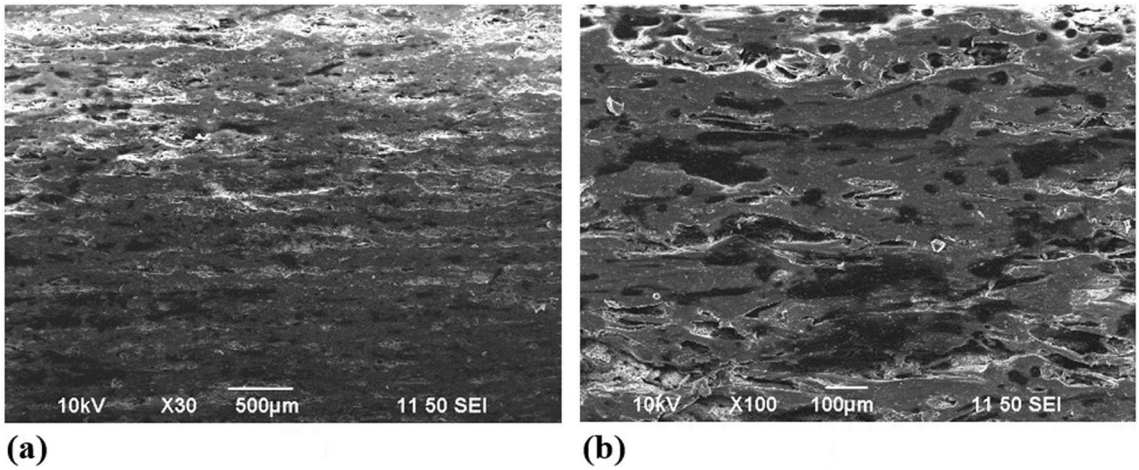


**Fig. 11** SEM images of the side surface of the PAHT-CF impact test specimen

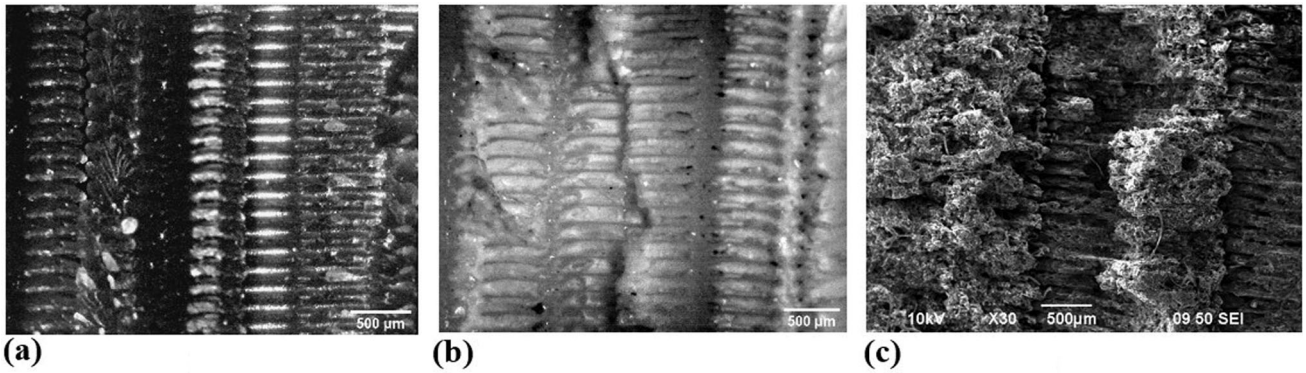


**Fig. 12** Representative images of the cross section after fracture of the impact test specimens: (a) optical image of PLA; (b) optical image of PC; (c) SEM image of PAHT-CF

clearly distinguished, while black regions with various geometries are also visible in Fig. 11(b). The larger voids represent surface irregularities created during the layer-upon-layer deposition and the heating and cooling process of the melted material. The smaller pores have a more regular geometry and have been created due to the absorption of moisture from the environment, as PAHT-CF is a hydrophobic material (Ref 49).

Figure 12 shows the deformation after fracture in the cross-sectional area of the impact test specimens. The layer-to-layer deposition is clearly visible. It is also possible to distinguish the printing beads in each layer for all specimens. Some vertical air gaps can be noticed, which represent inter-beads micro voids that were created during the infill pattern deposition. A brittle crack can be observed in the fracture surface of the PC

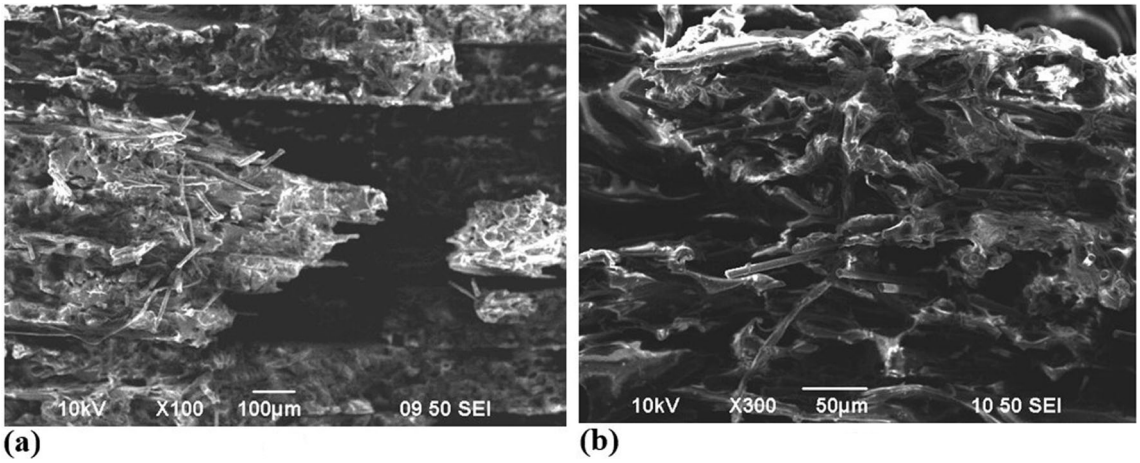


**Fig. 13** SEM images of the cross section after fracture of the PAHT-CF impact test specimen

specimen (Fig. 12b), which has been created in *Z*-axis perpendicular to the impact load direction. The fracture surface of PAHT-CF (Fig. 12c) is quite rough with sharp peaks, indicating a brittle fracture with evident ductile deformation perpendicular to the fractured surface.

SEM images of the fracture surface of the PAHT-CF impact test specimen are provided in Fig. 13. A close examination reveals broken carbon fibers protruding from the fractured surface of PAHT-CF. The black areas correspond to the valleys created on the rough surface due to the ductile deformation. The carbon fibers appear to be partially aligned with the direction of the printing beads, however their dispersion in the polyamide matrix is not uniform. Some fibers can be observed in Fig. 13(b) that have been broken right at the fracture surface and do not protrude from it, while others have been pulled-out. According to the images, the failure occurred due to the fiber breakage of fibers and the existence of gaps between the layers and the beads, that acted as crack points and led to crack propagation. The observations for PAHT-CF were similar to the results of the fractural analysis obtained by Condruz et al. (Ref 49).

## 5. Conclusions

The present research work investigates the physical and mechanical behavior of PLA, PC, and PAHT-CF specimens fabricated using the Fused Deposition Modeling printing technique and realistic conditions (same 3D printer, common process parameters and environmental conditions). The major objective and contribution of this study is to provide a complete comparative analysis of the mechanical properties through experimental tests, namely tensile, three-point bending, impact and creep testing, measurements of hardness, density and porosity, as well as optical microscopy and SEM observations for the morphology of the specimens.

The following conclusions are drawn:

- PAHT-CF printed specimens exhibit better tensile and flexural behavior than PLA and PC samples and a very good impact resistance, slightly lower than PC, despite the increased porosity. The selection of appropriate process parameters that reduce porosity, such as raster width and printing speed, could further improve the mechanical properties.
- Stage II creep resistance of PAHT-CF printed specimens was found to be superior to PLA and PC, however the effect of the process parameters in the creep behavior under a constant tensile load must be further investigated.
- The highest shore D hardness value was recorded for PLA specimens indicating that it is more brittle in comparison to PC and PAHT-CF which were found to be more ductile with respect to fracture.
- The morphology of the PAHT-CF printed specimens is very sensitive to the nozzle printing temperature and the printing speed, and these two parameters must be selected appropriately and relative to each other. A high printing temperature leads to good material fluidity, good bonding process and less intra-bead voids. However, a too high temperature together with a high speed impedes the cooling process, as the material does not have time to cool before a new layer is deposited, and this can cause interlayer defects and poor surface quality. On the other hand, a lower printing temperature can lead to smaller dimensional deviations but can also cause incomplete melting and reduce the adhesion of the material.
- Further work will be conducted to investigate the effect of printing temperature and printing speed on the dimensional accuracy, surface quality and porosity of PAHT-CF, as well as the effect of reinforcement fibers on the mechanical properties of polyamide printed specimens.

### Authors Contributions

SD and II were involved in methodology, validation, writing—original draft and writing—review and editing. SD, II and DRP were involved in investigation. DRP was involved in software. All authors have read and agreed to the published version of the manuscript.

## Funding

Open access funding provided by HEAL-Link Greece. This research was supported and funded by the Special Account for Research Grants of the University of West Attica.

## Conflict of interest

The authors declare no conflict of interest.



## References

1. S. Rouf, S. Raina, M.I. Hag, N. Naveed, S. Jeganmohan, and A.F. Kichloo, 3D Printed Parts and Mechanical Properties: Influencing Parameters, *Sustain. Aspects Global Market Scenar. Chall. Appl. Adv. Ind. Eng. Polym. Res.*, 2022, **5**(3), p 143–158. https://doi.org/10.1016/j.aiepr.2022.02.001
2. M. Harris, J. Potgieter, R. Archer, and K.M. Arif, Effect of Material and Process Specific Factors on the Strength of Printed Parts in Fused Filament Fabrication: A Review of Recent Developments, *Materials.*, 2019, **12**(10), p 1664. https://doi.org/10.3390/ma12101664
3. T.M. Medibew, A Comprehensive Review on the Optimization of the Fused Deposition Modeling Process Parameter for Better Tensile Strength of PLA-Printed Parts, *Adv. Mater. Sci. Eng.*, 2022 https://doi.org/10.1155/2022/5490831
4. A. Dey and N. Yodo, A Systematic Survey of FDM Process Parameter Optimization and Their Influence on Part Characteristics, *J. Manuf. Mater. Process.*, 2019, **3**(3), p 64. https://doi.org/10.3390/jmmp3030064
5. I.J. Solomon, P. Sevvel, and J. Gunasekaran, A Review on the Various Processing Parameters in FDM, *Mater. Today Proceed.*, 2021, **1**(37), p 509–514. https://doi.org/10.1016/j.matpr.2020.05.484
6. X. Peng, M. Zhang, Z. Guo, L. Sang, and W. Hou, Investigation of Processing Parameters on Tensile Performance for FDM-Printed Carbon Fiber Reinforced Polyamide 6 Composites, *Compos. Commun.*, 2020, **1**(22), p 100478. https://doi.org/10.1016/j.coco.2020.100478
7. N. Vidakis, M. Petousis, C.N. David, D. Sagris, N. Mountakis, and E. Karapidakis, Mechanical Performance over Energy Expenditure in MEX 3D Printing of Polycarbonate: A Multiparametric Optimization with the Aid of Robust Experimental Design, *J. Manuf. Mater. Process.*, 2023, **7**(1), p 38. https://doi.org/10.3390/jmmp7010038
8. S. Wickramasinghe, T. Do, and P. Tran, FDM-Based 3D Printing of Polymer and Associated Composite: A Review on Mechanical Properties, Defects and Treatments, *Polymers*, 2020, **12**(7), p 1529. https://doi.org/10.3390/polym12071529
9. X. Zhang, W. Fan, and T. Liu, Fused Deposition Modeling 3D Printing of Polyamide-Based Composites and its Applications, *Compos. Commun.*, 2020, **1**(21), p 100413. https://doi.org/10.1016/j.coco.2020.100413
10. J. Li, Y. Durandet, X. Huanga, G. Sunb, and D. Ruan, Additively Manufactured Fiber-Reinforced Composites: A Review of Mechanical Behavior and Opportunities, *J. Mater. Sci. Technol.*, 2022, **119**, p 219–244. https://doi.org/10.1016/j.jmst.2021.11.063
11. J.M. Chacón, M.A. Caminero, E. García-Plaza, and P.J. Núñez, Additive Manufacturing of PLA Structures using Fused Deposition Modelling: Effect of Process Parameters on Mechanical Properties and their Optimal Selection, *Mater. Des.*, 2017, **124**, p 143–157. https://doi.org/10.1016/j.matdes.2017.03.065
12. M.H. Hsueh, C.J. Lai, C.F. Chung, S.H. Wang, W.C. Huang, C.Y. Pan, Y.S. Zeng, and C.H. Hsieh, Effect of Printing Parameters on the Tensile Properties of 3D-Printed Polylactic Acid (PLA) Based on Fused Deposition Modeling, *Polymers*, 2021, **13**(14), p 2387. https://doi.org/10.3390/polym13142387
13. L. Marsavina, C. Vălean, M. Mărghitas, E. Linul, N. Razavi, F. Berto, and R. Brighenti, Effect of the Manufacturing Parameters on the Tensile and Fracture Properties of FDM 3D-Printed PLA Specimens, *Eng. Fract. Mech.*, 2022, **15**(274), p 108766. https://doi.org/10.1016/j.engfracmech.2022.108766
14. J. Singh, K.K. Goyal, and R. Kumar, Effect of Filling Percentage and Raster Style on Tensile Behavior of FDM Produced PLA Parts at Different Build Orientation, *Mater. Today Proceed.*, 2022, **63**, p 433–439. https://doi.org/10.1016/j.matpr.2022.03.444
15. D.G. Zisopol, I. Nae, A.-I. Portoaca, and I. Ramadan, A Statistical Approach of the Flexural Strength of PLA and ABS 3D Printed Parts, *Eng. Technol. Appl. Sci. Res.*, 2022, **12**, p 8248–8252. https://doi.org/10.48084/etasr.4739
16. B. Kartikeyan, A. Ponshanmugakumar, G. Saravanan, S. BharathGanesh, and V. Hemamalini, Experimental and Theoretical Analysis of FDM AM PLA Mechanical Properties, *Mater. Today Proceed.*, 2023 https://doi.org/10.1016/j.matpr.2023.05.105
17. P.K. Mishra, P. Senthil, S. Adarsh, and M.S. Anoop, An Investigation to Study the Combined Effect of Different Infill Pattern and Infill Density on the Impact Strength of 3D Printed Polylactic Acid Parts, *Compos. Commun.*, 2021, **1**(24), p 100605. https://doi.org/10.1016/j.coco.2020.100605
18. S. Bardiya, J. Jerald, and V. Satheeshkumar, Effect of Process Parameters on the Impact Strength of Fused Filament Fabricated (FFF) Polylactic acid (PLA) Parts, *Mater. Today Proceed.*, 2021, **41**, p 1103–1106. https://doi.org/10.1016/j.matpr.2020.08.066
19. A.A. Ansari and M. Kamil, Izod Impact and Hardness Properties of 3D Printed Lightweight CF-Reinforced PLA Composites using Design of Experiment, *Int. J. Lightweight Mater. Manuf.*, 2022, **2**, p 369–383. https://doi.org/10.1016/j.ijlmm.2022.04.006
20. M.M. Hanon, J. Dobos, and L. Zsidai, The Influence of 3D Printing Process Parameters on the Mechanical Performance of PLA Polymer and its Correlation with Hardness, *Proced. Manuf.*, 2021, **54**, p 244–249. https://doi.org/10.1016/j.promfg.2021.07.038
21. G.Y. Dakhil, R.M. Salih, and A.M. Hameed, Influence of Infill Pattern, Infill Ratio on Compressive Strength and Hardness of 3D Printed Polylactic Acid (PLA) Based Polymer, *J. Appl. Sci. Nanotechnol.*, 2023, **3**(1), p 1–7. https://doi.org/10.53293/jasn.2022.4745.1141
22. M. Waseem, B. Salah, T. Habib, W. Saleem, M. Abas, R. Khan, U. Ghani, and M.U. Siddiqi, Multi-Response Optimization of Tensile Creep Behavior of PLA 3D Printed Parts Using Categorical Response Surface Methodology, *Polymers*, 2020, **12**(12), p 2962. https://doi.org/10.3390/polym12122962
23. M.R. Adibeig, F. Vakili-Tahami, and M.A. Saeimi-Sadigh, Numerical and Experimental Investigation on Creep Response of 3D Printed Polylactic acid (PLA) Samples Part I The Effect of Building Direction and Unidirectional Raster Orientation, *J. Mech. Behavior Biomed. Mater.*, 2023, **1**(145), p 106025. https://doi.org/10.1016/j.jmbbm.2023.106025
24. H. Van de Vries, R. Engelen, and E. Janssen, Impact Strength of 3D-Printed Polycarbonate, *Electron. Energ.*, 2020, **33**(1), p 105–117. https://doi.org/10.2298/FUEE2001105V
25. K. Bulanda, M. Oleksy, R. Oliwa, G. Budzik, Ł Przeszłowski, J. Fal, and T. Jesionowski, Polymer Composites Based on Polycarbonate (PC) Applied to Additive Manufacturing Using Melted and Extruded Manufacturing (MEM) Technology, *Polymers*, 2021, **13**(15), p 2455. https://doi.org/10.3390/polym13152455
26. N. Vidakis, M. Petousis, E. Velidakis, M. Spiridaki, and J.D. Kechagias, Mechanical Performance of Fused Filament Fabricated and 3D-Printed Polycarbonate Polymer and Polycarbonate/Cellulose Nanofiber Nanocomposites, *Fibers.*, 2021, **9**(11), p 74. https://doi.org/10.3390/fib9110074

27. A. Bahar, S. Belhabib, S. Guessasma, F. Benmahiddine, A.E. Hamami, and R. Belarbi, Mechanical and Thermal Properties of 3D Printed Polycarbonate, *Energies*, 2022, **15**(10), p 3686. https://doi.org/10.3390/en15103686
28. F. Faroze, V. Srivastava, and A. Batish, Enhancing Mechanical Properties of Polycarbonate Parts Developed by Fused Filament Fabrication using RSM-Topsis Hybrid Approach, *Polym. Eng. Sci.*, 2023, **63**(12), p 4186–4206. https://doi.org/10.1002/pen.26517
29. A.G. Salazar-Martín, M.A. Pérez, A.A. García-Granada, G. Reyes, and J.M. Puigoriol-Forcada, A Study of Creep in Polycarbonate Fused Deposition Modelling Parts, *Mater. Des.*, 2018, **5**(141), p 414–425. https://doi.org/10.1016/j.matdes.2018.01.008
30. J.M. Chacón, M.A. Caminero, P.J. Núñez, E. García-Plaza, I. García-Moreno, and J.M. Reverte, Additive Manufacturing of Continuous Fibre Reinforced Thermoplastic Composites using Fused Deposition Modelling: Effect of Process Parameters on Mechanical Properties, *Compos. Sci. Technol.*, 2019, **8**(181), p 107688. https://doi.org/10.1016/j.compscitech.2019.107688
31. M. Mohammadizadeh, A. Imeri, I. Fidan, and M.J. Elkelany, 3D Printed Fiber Reinforced Polymer Composites-Structural Analysis, *Compos. Part B Eng.*, 2019, **15**(175), p 107112. https://doi.org/10.1016/j.compositesb.2019.107112
32. S. Dul, L. Fambri and A. Pegoretti, High-Performance Polyamide/Carbon Fiber Composites for Fused Filament Fabrication: Mechanical and Functional Performances, *J. Mater. Eng. Perform. Addit. Manuf.*, 2021, **30**, p 5066–5085. https://doi.org/10.1007/s11665-021-05635-1
33. M. Tutar, A Comparative Evaluation of the Effects of Manufacturing Parameters on Mechanical Properties of Additively Manufactured PA and CF-Reinforced PA Materials, *Polymers*, 2022, **15**(1), p 38. https://doi.org/10.3390/polym15010038
34. B. Sun, S. Mubarak, G. Zhang, K. Peng, X. Hu, Q. Zhang, L. Wu, and J. Wang, Fused-Deposition Modeling 3D Printing of Short-Cut Carbon-Fiber-Reinforced PA6 Composites for Strengthening, Toughening, and Light Weighting, *Polymers*, 2023, **15**(18), p 3722. https://doi.org/10.3390/polym15183722
35. F. Calignano, M. Lorusso, I. Roppolo, and P. Minetola, Investigation of the Mechanical Properties of a Carbon Fibre-Reinforced Nylon Filament for 3D Printing, *Machines.*, 2020, **8**(3), p 52. https://doi.org/10.3390/machines8030052
36. Ł Pejkowski, J. Seyda, K. Nowicki, and D. Mrozik, Mechanical Performance of Non-reinforced, Carbon Fiber Reinforced and Glass Bubbles Reinforced 3D Printed PA12 Polyamide, *Polym. Test.*, 2023, **15**(118), p 107891. https://doi.org/10.1016/j.polymertesting.2022.107891
37. N.G. Tanikella, B. Wittbrodt, and J.M. Pearce, Tensile Strength of Commercial Polymer Materials for Fused Filament Fabrication 3D Printing, *Addit. Manuf.*, 2017, **15**, p 40–47. https://doi.org/10.1016/j.addma.2017.03.005
38. M. Lay, N.L. Thajudin, Z.A. Hamid, A. Rusli, M.K. Abdullah, and R.K. Shuib, Comparison of Physical and Mechanical Properties of PLA, ABS and Nylon 6 Fabricated using Fused Deposition Modeling and Injection Molding, *Compos. Part B Eng.*, 2019, **1**(176), p 107341. https://doi.org/10.1016/j.compositesb.2019.107341
39. S. Kannan and M. Ramamoorthy, Mechanical Characterization and Experimental Modal Analysis of 3D Printed ABS, PC and PC-ABS Materials, *Mater. Res. Express.*, 2020, **7**(1), p 015341. https://doi.org/10.1088/2053-1591/ab6a48
40. N. Vidakis, M. Petousis, E. Velidakis, M. Liebscher, V. Mechtcherine, and L. Tzounis, On the Strain Rate Sensitivity of Fused Filament Fabrication (FFF) Processed PLA, ABS, PETG, PA6, and PP Thermoplastic Polymers, *Polymers*, 2020, **12**(12), p 2924. https://doi.org/10.3390/polym12122924
41. N. Arunkumar, N. Sathishkumar, S.S. Sanmugapriya, and R. Selvam, Study on PLA and PA Thermoplastic Polymers Reinforced with Carbon Additives by 3D Printing Process, *Mater. Today Proceed.*, 2021, **46**, p 8871–8879. https://doi.org/10.1016/j.matpr.2021.05.041
42. R.A. García-León, M. Rodríguez-Castilla, and W. Quintero, Experimental Analysis of Impact Resistance of 3D Polycarbonate and Nylon + Carbon Fiber Specimens, *J. Mater. Eng. Perform.*, 2021 https://doi.org/10.1007/s11665-020-05422-4
43. O. Dogan, Short-term Creep Behaviour of Different Polymers Used in Additive Manufacturing under Different Thermal and Loading Conditions, *J. Mech. Eng.*, 2022, **68**, p 451–460. https://doi.org/10.5545/sv-jme.2022.191
44. P. Frohn-Sörensen, M. Geueke, B. Engel, B. Löffler, P. Bickendorf, A. Asimi, G. Bergweiler, and G. Schuh, Compressive and Flexural Material Properties of PC, PLA, PA and PETG for Additive Tooling in Sheet Metal Forming, (2022), https://doi.org/10.31224/2239
45. S.L. Rodríguez-Reyna, C. Mata, J.H. Díaz-Aguilera, H.R. Acevedo-Parra, and F. Tapia, Mechanical properties optimization for PLA, ABS and Nylon+ CF manufactured by 3D FDM printing, *Mater. Today Commun.*, 2022, **1**(33), p 104774. https://doi.org/10.1016/j.mtcomm.2022.104774
46. P.A. Palacios, A. Velazquez, R. Zelaya, and A.E. Patterson, Shore Hardness of as-Printed and Dehydrated Thermoplastic Materials Made using Fused Filament Fabrication (FFF), *Mater. Today Commun.*, 2023, **1**(35), p 105971. https://doi.org/10.1016/j.mtcomm.2023.105971
47. R. Venkatesh, J.J.J. Britto, K. Amudhan, V. Anbumalar, R. Prabhakaran, and R.T. Sakthi, Experimental Investigation of Mechanical Properties on CF Reinforced PLA, *ABS Nylon Compos. Part Mater. Today Proceed.*, 2023, **76**, p 647–653. https://doi.org/10.1016/j.matpr.2022.12.091
48. A. Yankin, Y. Alipov, A. Temirgali, G. Serik, S. Danenova, D. Talamona, and A. Perveen, Optimization of Printing Parameters to Enhance Tensile Properties of ABS and Nylon Produced by Fused Filament Fabrication, *Polymers*, 2023, **15**(14), p 3043.
49. M.R. Condruz, A. Paraschiv, T.A. Badea, D. Useriu, T.F. Frigioescu, G. Badea, and G. Cican, A Study on Mechanical Properties of Low-Cost Thermoplastic-Based Materials for Material Extrusion Additive Manufacturing, *Polymers*, 2023, **15**(14), p 2981. https://doi.org/10.3390/polym15142981
50. D. Syrlybayev, B. Zharylkassyn, A. Seisekulova, M. Akhmetov, A. Perveen, and D. Talamona, Optimisation of Strength Properties of FDM Printed Parts—A Critical Review, *Polymers*, 2021, **13**(10), p 1587. https://doi.org/10.3390/polym13101587
51. A. Chadha, M.I.U. Haq, A. Raina, R.R. Singh, N.B. Penumarti, and M.S. Bishnoi, Effect of Fused Deposition Modelling Process Parameters on Mechanical Properties of 3D Printed Parts, *World J. Eng.*, 2019, **16**, p 550–559. https://doi.org/10.1108/WJE-09-2018-0329
52. S. Tandon, R. Kacker, and K.G. Sudhakar, Experimental Investigation on Tensile Properties of the Polymer and Composite Specimens Printed in a Triangular Pattern, *J. Manuf. Process.*, 2021, **68**, p 706–715. https://doi.org/10.1016/j.jmapro.2021.05.074
53. K.E. Aslani, D. Chaidas, J. Kechagias, P. Kyratsis, and K. Salonitis, Quality Performance Evaluation of Thin-Walled PLA 3D Printed Parts Using the Taguchi Method and Grey Relational Analysis, *J. Manuf. Mater. Proc.*, 2020, **4**(47), p 1–17. https://doi.org/10.3390/jmmp4020047
54. N. Jia, and V.A. Kagan, Mechanical Performance of Polyamides with Influence of Moisture and Temperature—Accurate Evaluation and Better Understanding. In book: Plastics Failure Analysis and Prevention, (2021), pp. 95-104, https://doi.org/10.1016/B978-188420792-1.50014-7
55. G. Liao, Z. Li, H. Cheng, D. Xu, D. Zhu, S. Jiang, J. Guo, X. Chen, G. Xu, and Y. Zhu, Properties of Oriented Carbon Fiber/Polyamide 12 Composite Parts Fabricated by Fused Deposition Modeling, *Mater. Des.*, 2018, **139**, p 283–292. https://doi.org/10.1016/j.matdes.2017.11.027
56. Y. Tao, F. Kong, Z. Li, J. Zhang, X. Zhao, Q. Yin, D. Xing, and P. Li, A Review on Voids of 3D Printed Parts by Fused Filament Fabrication, *J. Market. Res.*, 2021, **15**, p 4860–4879. https://doi.org/10.1016/j.jmrt.2021.10.108
57. S. Kumar, S. Teraiya, and Y. Potdar, Experimental Investigation on Porosity and Flexural Strength of Polymer Parts Fabricated by Fused Deposition Modeling, *Polym. Eng. Sci.*, 2023, **63**, p 531–545. https://doi.org/10.1002/pen.26227